

ASSESSMENT OF THE IMPACTS OF RADIO FREQUENCY INTERFERENCE ON SMAP RADAR AND RADIOMETER MEASUREMENTS

Curtis W. Chen,¹ Jeffrey R. Piepmeier,² Joel T. Johnson,³ Hiram Ghaemi¹

¹Jet Propulsion Laboratory, California Institute of Technology

²NASA GSFC

³Ohio State University

ABSTRACT

The NASA Soil Moisture Active and Passive (SMAP) mission will measure soil moisture with a combination of L-band radar and radiometer measurements. We present an assessment of the expected impact of radio frequency interference (RFI) on SMAP performance, incorporating projections based on recent data collected by the Aquarius and SMOS missions. We discuss the impacts of RFI on the radar and radiometer separately given the differences in (1) RFI environment between the shared radar band and the protected radiometer band, (2) mitigation techniques available for the different measurements, and (3) existing data sources available that can inform predictions for SMAP.

Index Terms— Soil moisture remote sensing, microwave radar, microwave radiometry, radio frequency interference

1. INTRODUCTION

NASA's Soil Moisture Active and Passive (SMAP) mission [1], scheduled for launch in late 2014, includes L-band radar and radiometer systems to measure soil moisture. Corruption of science data by radio frequency interference (RFI) is a significant concern, particularly given recent experience with the SMOS and Aquarius L-band radiometer systems and the PALSAR L-band radar system. To address these concerns, the SMAP mission has been performing RFI risk assessment activities and has incorporated RFI mitigation approaches into the SMAP instrument designs. This paper provides an update on SMAP RFI risk assessment activities, as well as information on SMAP RFI mitigation strategies and status.

2. RADAR RFI ASSESSMENT

The RFI assessment for the SMAP radar is based on simulation, with the simulation methodology validated through comparison with Aquarius radar data.

The radar RFI simulation employs models of ground-based emitters with various signal characteristics operating in the 1215–1300 MHz radar band in order to capture the

RFI environment. Each simulation run assumes a particular set of ground emitters at specified geographic locations and with specified peak power levels, center frequencies, bandwidths, duty cycles, antenna patterns, etc. Emitter characteristics are varied in different runs of the simulation to assess sensitivities. Unfortunately, we have reliable information on pulsed, terrestrial emitters only for North America. Our radar RFI predictions are therefore based on simulations over North America and are extrapolated globally as described below.

Models for the SMAP radar in the simulation are based on lab measurements of brassboard radar hardware, design analyses of the SMAP antenna patterns, etc. The simulation computes the characteristics of RFI as observed by the SMAP radar in the time domain. At each simulation time step, the simulation evaluates link calculations between the SMAP radar and each interfering source, propagating both the state of the rotating SMAP antenna over the spacecraft orbit and the states of the ground emitters between successive time steps.

The simulation methodology has been validated through comparison to real RFI observed by the Aquarius radar [2]. That is, when Aquarius parameters are assumed in the simulation, the RFI statistics of the simulated results compare favorably to those of real Aquarius measurements. While these results are strictly valid only over North America because of the limitations on our knowledge of emitter characteristics, the global variation in the real Aquarius data can be used to extrapolate the simulated results to the rest of the world through artificial changes in the assumed emitter environment. Figure 1 shows a comparison of real and simulated Aquarius data over North America, and real Aquarius data over parts of Europe and Asia chosen for their noisy RFI environments. The corresponding real and simulated data curves agree very well. Global variations in the real data are significant, but not extreme, particularly over the medium-power regime of most interest to SMAP.

The SMAP simulation extends beyond the calculation of RFI power levels at the SMAP radar receiver, however. In order to model the end-to-end SMAP radar measurement, the simulation incorporates models for the various mechanisms by which RFI in the radar data causes errors in

the eventual radiometric measurements, including the effects of ground processing that includes RFI mitigation algorithms. That is, the simulation assumes that RFI with particular characteristics can be detected and excised during ground processing as described in earlier work [3]; it subsequently models the errors arising from undetected RFI and from the effects of data excision itself. In particular, the simulation computes the errors from (1) undetected RFI in the radar signal channels, (2) undetected RFI in the radar noise-estimation channels, (3) degradation of the measurement integrated sidelobe ratio due to RFI excision, (4) increased K_{pc} error due to RFI excision, and (5) receiver compression. The simulation also estimates the fraction of data lost due to the presence of excessive RFI.

The simulation results suggest that the RFI-mitigation techniques currently planned for the SMAP radar will be sufficient to achieve the level of radar performance expected. Figure 2 shows an example of the cumulative distribution function (CDF) of simulated radiometric errors over time in a set of SMAP radar measurements under nominal assumptions on the emitter environment, the instrument parameters, etc. While the distribution has a long tail, over 98% of the measurements have errors within the 0.4 dB allocation to RFI-induced errors in the current error budget (denoted by the vertical dashed line). Figure 3 shows a time-domain plot of the corresponding RFI-induced radiometric errors from the simulation. The six horizontal clusters of data represent six concatenated spacecraft passes over North America at different longitudes. Although the visual appearance of the plot is dominated by the high temporal variability of the errors and long tails of the error distribution given the large number of measurements represented on the horizontal axis, the mean and RMS errors taken over two-minute sliding windows in time are still within the error allocation.

3. RADIOMETER RFI ASSESSMENT

The RFI assessment methodology for the radiometer is based on comprehensive testing of instrument hardware under artificial and realistic conditions. Whilst said hardware is unavailable, recent efforts have been focused on analysis of the RFI impact on SMOS [4] and Aquarius [5] radiometer data to elucidate changes to the current understanding of the statistical RFI environment, which is based on SMAPVEX08 [6] airborne results. Several previous works have reported analyses of SMOS RFI (e.g. [7]-[11]) so that Aquarius datasets (available since August 2011) are highlighted in what follows.

Figure 4 (upper) illustrates Aquarius radiometer “max-hold” brightness temperatures (over the three antenna beams of incidence angle 28.7, 37.8, and 45.6 degrees respectively) for North American observations from November-December 2011. As with SMOS, significant RFI is observed; it is notable that North America is regarded as more “quiet” than other global regions. It is also important

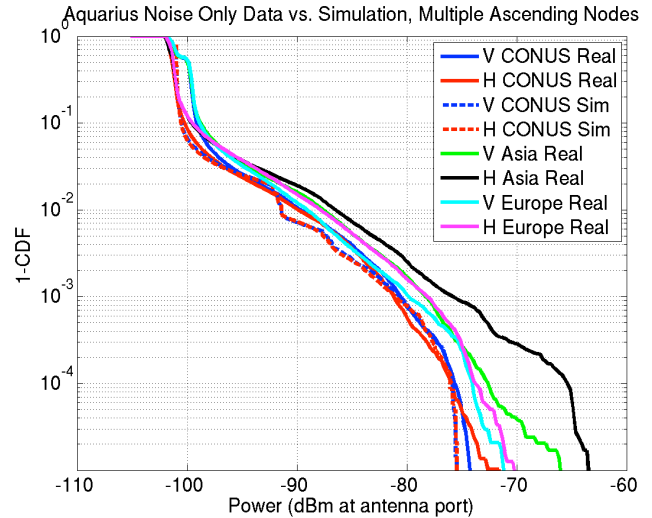


Figure 1. Complementary cumulative distribution functions of real and simulated Aquarius radar noise-only data for sets of passes over different geographical regions. Power levels above the radar noise floor are due to RFI.

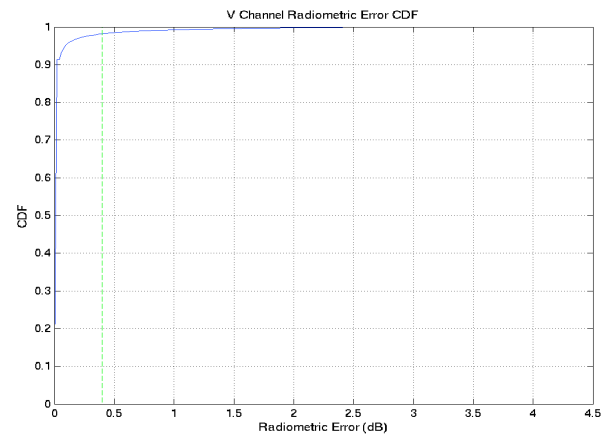


Figure 2. Cumulative distribution function of radiometric errors due to RFI in the SMAP radar measurement after mitigation based on a simulation with nominal assumptions on system parameters and the emitter environment.

to note that images of this sort, while very sensitive to large RFI sources, are not useful for observing the low-level sources of most concern for science. Because Aquarius has a pulse-detection algorithm operating on its 10 ms internal data, it is possible to mitigate pulse-type interference. Figure 4 (lower) illustrates the max-hold brightnesses after the mitigation process. A clear reduction of corruption is observed, indicating that many of the sources in the left image are pulsed emissions. However some large brightnesses remain, likely associated with more continuous emissions. Continued studies of both the Aquarius and

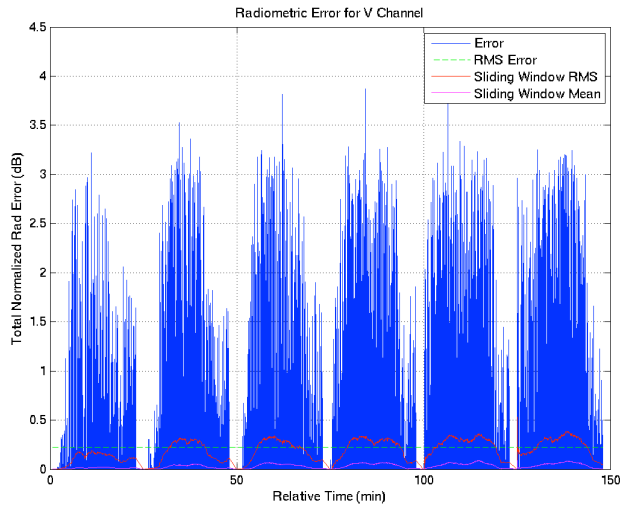


Figure 3. Time-domain plot of simulated RFI-induced radar errors corresponding to the CDF of Fig. 2. Each time step corresponds to 30 ms. The high temporal variability and long tails of the error distribution are noteworthy and dominate the visual appearance of the plot, but the overall error statistics are within the current allocation.

SMOS datasets are in progress to improve knowledge of the RFI environment for SMAP planning.

The SMAP radiometer has been designed to be capable of a variety of approaches for RFI mitigation [12], including “pulse” [13], “cross-frequency” [14], and “kurtosis” [15] RFI detection methods, and includes an RFI excision methodology based on the availability of 16 frequency channels at approximately 1 ms time resolution. Simulation tests of this architecture utilizing RFI environment statistics obtained from Aquarius and SMOS show that mitigation is expected to be achieved that meets science requirements for SMAP data products.

Figure 5 illustrates an example from the performance simulation. Given an assumed RFI type (in this example, $2 \mu\text{s}$ pulsed CW interference producing a specified brightness temperature contribution if not mitigated), the RFI bias remaining following the application of SMAP mitigation algorithms can be obtained from Monte Carlo simulations. The curves in Fig. 5 illustrate the dependence of this bias on the RFI amplitude. An integration of these errors over an estimated probability density function of global RFI amplitudes (also shown in Fig. 5, and obtained from satellite data analysis) enables the globally averaged errors to be estimated. This process remains dependent on the source type modeled; repeated simulations are being performed for a variety of potential source types to quantify performance and refine mitigation algorithms.

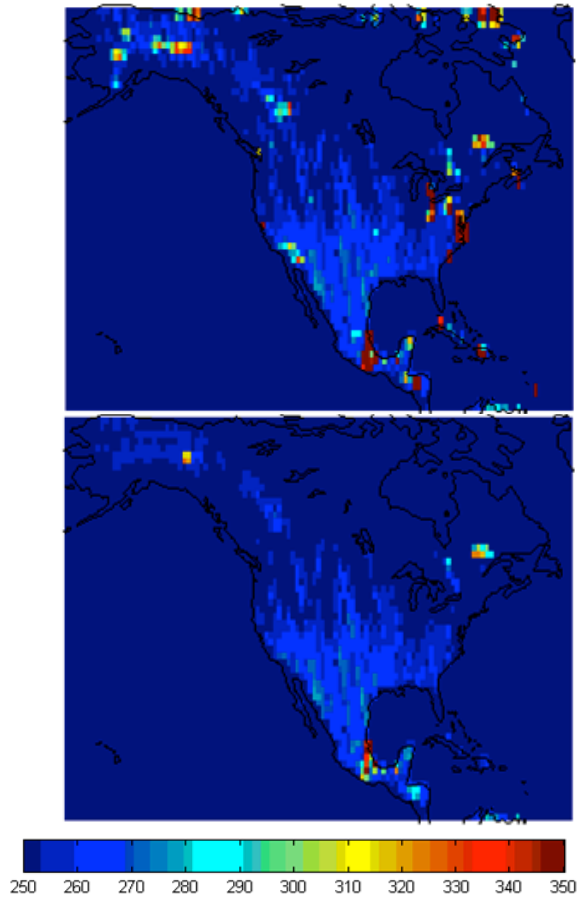


Figure 4. “Max hold” of Aquarius horizontally polarized brightness temperatures over North America, Nov-Dec 2011; (upper) prior to application of RFI mitigation (lower) after application of RFI mitigation.

Hardware testing remains the primary means of assessing radiometer performance in the presence of RFI. Radiometer RF and digital electronics engineering model hardware is currently undergoing integration and testing, and comprehensive RFI tests are included as part of this process. This testing will include exposing the radiometer to both continuous wave (CW) and pulsed interference over a broad range of well controlled frequencies, power levels, and duty cycles as well as a realistic environment based on various modulation schemes and power levels. A prediction of on-orbit performance will then be made by synthesizing an error CDF based upon combining the test results with the aforementioned environmental prediction from SMOS and Aquarius.

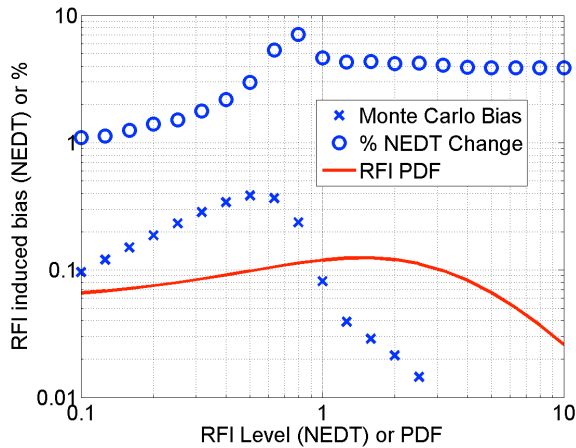


Figure 5. Conceptual description of SMAP Radiometer RFI performance simulation. The symbols represent remaining RFI bias and percent change in NEDT from simulated SMAP radiometer outputs post-mitigation for an assumed $2 \mu\text{s}$ pulsed-CW interference type. The red curve is an estimate of the global PDF of RFI amplitudes obtained from satellite data analysis. Integration of the RFI bias over the PDF in this particular example shows a globally averaged RFI error of approximately 0.04 K.

4. CONCLUSIONS

In implementing the SMAP mission, a multi-layer strategy has been adopted in order to minimize errors due to RFI. The instrument hardware has been designed with robustness to RFI as an explicit objective. Ground processing will further mitigate RFI through detection and/or excision of unwanted interference. Finally, residual errors due to RFI have been assumed in high-level error budgets.

In order to evaluate the efficacy of this end-to-end RFI strategy, the RFI environments for both the SMAP radar and radiometer have been assessed through examination of data from Aquarius and SMOS. These assessments have been fed into models for the SMAP hardware and mitigation approaches, and the results indicate that SMAP will be able to achieve its science objectives in the presence of RFI.

5. ACKNOWLEDGEMENTS

A portion of the work described in this paper was carried out by the Jet Propulsion Laboratory, California Institute of Technology under a contract with the National Aeronautics and Space Administration. Aquarius data were furnished through the NASA/CONAE Aquarius/SAC-D Project.

6. REFERENCES

[1] D. Entekhabi et al, "The Soil Moisture Active Passive (SMAP) mission," *Proc. IEEE*, vol. 98, pp. 704-716, 2010.

[2] D.M. Le Vine, G.S.E. Lagerloef, R. Colomb, S. Yueh, F. Pellerano, "Aquarius: An Instrument to Monitor Sea Surface

Salinity From Space," *IEEE Trans. Geosci. Rem. Sens.*, vol 45 (#7), pp 2040-2050, July, 2007.

[3] S. Chan, M. Fischman, M. Spencer, "RFI mitigation and detection for the SMAP radar," *Proc. IGARSS 2011*, Vancouver, Canada.

[4] Special issue on Soil Moisture and Ocean Salinity (SMOS) mission, *IEEE Trans. Geosci. Rem. Sens.*, Vol50 (#5, part 1), May 2012.

[5] Lagerloef, G. et al, "The Aquarius SAC-D mission," *Oceanography*, vol. 21, pp. 68–81, 2008.

[6] J. Park et al, "Airborne L-band RFI observations from the SMAPVEX08 campaign and associated flights," *IEEE Trans. Geosci. Rem. Sens.*, vol. 49, pp. 3359-3370, 2011.

[7] Camps, A., J. Gourrion, J. M. Tarongi, A. Gutierrez, J. Barbosa, and R. Gutierrez, "RFI analysis in SMOS imagery," *Proc IGARSS 2010*, Honolulu, Hawaii.

[8] Anterrieu, E., "On the detection and quantification of RFI in L1A signals provided by SMOS," *IEEE Trans. Geosci. Rem. Sens.*, vol. 49, pp. 3986–3992, 2010.

[9] J. T. Johnson and M. Aksoy, "Studies of radio frequency interference in SMOS observations," *Proc IGARSS 2011*, Vancouver, Canada.

[10] Misra, S.; Ruf, C. S.; , "Analysis of Radio Frequency Interference Detection Algorithms in the Angular Domain for SMOS," *IEEE Trans. Geosci. Rem. Sens.*, vol. 50, pp. 1448–1457, 2012.

[11] R. Oliva et al, "SMOS RFI scenario: status and actions taken to improve the RFI environment in the 1400-1427 MHz passive band," *IEEE Trans. Geosci. Rem. Sens.*, vol. 50, pp. 1427–1440, 2012.

[12] R. Castro, A. Gutierrez, and J. Barbosa, "A first set of techniques to detect RFI and mitigate their impact on SMOS data," *IEEE Trans. Geosci. Rem. Sens.*, vol. 50, pp. 1440–1447, 2012.

[13] M. Spencer et al, "The SMAP mission L-band radar/radiometer instrument," *Proc. IGARSS 2010*, pp. 3240–3243, 2010.

[14] J. T. Johnson and L. C. Potter, "A study of detection algorithms for pulsed sinusoidal interference in microwave radiometry," *IEEE Trans. Geosci. Rem. Sens.*, vol. 47, pp. 628–636, 2009.

[15] B. Guner and J. T. Johnson, "Performance study of a cross-frequency detection algorithm for pulsed sinusoidal RFI in microwave radiometry," *IEEE Trans. Geosci. Rem. Sens.*, vol. 48, pp. 2899–2908, 2010.

[16] C. S. Ruf, S. M. Gross, S. Misra, "RFI detection and mitigation for microwave radiometry with an agile digital detector," *IEEE Trans. Geosci. Rem. Sens.*, vol. 44, pp. 694–706, 2006.